Inertial Instability and Mesoscale Convective Systems. Part II: Symmetric CISK in a Baroclinic Flow

KERRY A. EMANUEL[1]

Department of Atmospheric Sciences, University of California, Los Angeles 90024

(Manuscript received 29 June 1981, in final form 25 January 1982)

ABSTRACT

Numerous budget studies of organized persistent systems of convective clouds outside the tropics suggest that circulations of mesoscale proportions are important in supplying moisture to the convective clouds, though the dynamical nature of *mesoscale* flows remains poorly defined. In Part I (Emanuel, 1979, hereafter referred to as Part I) it is demonstrated that circulations resulting from symmetric instability of shear flows in rotating fluids have a fundamentally *mesoscale* character in that both ambient rotation and ageostrophic advection are necessary for instability. The results of Part I are here extended to include the effects of latent heat release in a conditionally unstable atmosphere, using the formalism of the CISK approach. It is found that the presence of shear parallel to the wave fronts introduces new wave-CISK modes which are not strongly dependent on the specified vertical structure of the cumulus heating. The new baroclinic modes are of mesoscale dimensions, have growth rates proportional to the vertical shear of the ambient flow and propagate toward the warm air. These modes compare favorably with observations of squall lines within baroclinic flows.

1. Introduction

The interaction of convective clouds with circulations of larger scale has been an important subject of research in recent years. While the development of individual cumulus clouds may depend on the local convective instability of the large-scale environment, the character of ensembles of cumulus clouds depends crucially on the presence of circulations of fundamentally larger scale. In the tropics, the development of ensembles of cumulus clouds appears to proceed in such a way that the stabilization of the environment by the convection keeps pace with the destabilization effected by large-scale processes, as proposed by Arakawa and Shubert (1974). In some cases, the convective clouds interact constructively with larger-scale circulations to produce systems of great intensity and longevity, as embodied in the CISK theory of tropical cyclone development (Charney and Eliassen, 1964).

Outside the tropics, many severe convective events occur within strongly baroclinic flows and may also be associated with ensembles with lifetimes much greater than those typical of individual convective cells. Budget studies (e.g., Fritsch *et al.*, 1976) as well as practical forecasting experience show that these too are supported by circulations of larger scale, but very frequently this larger scale cannot be immediately identified with patterns of vertical velocity associated with traveling baroclinic waves. Hales (1979) suggests, for example, that there is often little correlation between vorticity advection at 250 mb and severe storm occurrence.

The failure to identify the development of many convective systems with quasi-geostrophically describable fields of vertical motion led immediately to the proposition that such systems are initiated and/or sustained by circulations of a scale intermediate between the synoptic and cumulus scales. The origin and history of the term *mesoscale*, as applied to these systems, has recently been reviewed by Fujita (1981); the definition of the term has heretofore been based almost solely on observations. Research on the mechanism of frontogenesis (e.g., Hoskins and Bretherton, 1972) suggests a dynamical significance of *mesoscale*; *viz.*, that both Coriolis accelerations and ageostrophic advection are necessary to these circulations. Stated simply, mesoscale circulations of this type are characterized by a Rossby number of order unity. In Part I it is shown that symmetric instability also leads to circulations which conform to this dynamical definition of mesoscale.

While the mesoscale organization of convection is sometimes clearly attributable to such largely independent circulations as fronts (Newton, 1950), drylines (Fawbush *et al.*, 1951), and sea breezes (Cotton *et al.*, 1976), there exist some cases for which it is difficult to identify a pre-existing mesoscale circu-

[1] Present affiliation: Department of Meteorology and Physical Oceanography, Massachusetts Institute of Technology, Cambridge 02139.

0022-4928/82/051080-18$08.50

lation. Such is the case of pre-coldfrontal squall lines, which often develop in regions removed from existing fronts (Fulks, 1951). It is intriguing to consider the possibility that such mesoscale systems are self-exciting and involve a CISK-like cooperative interaction between the cumulus and the mesoscale.

Investigations of the CISK mechanism have concerned the maintenance of cumulus clouds by moisture convergence associated with either Ekman pumping, as in tropical cyclones, or with inviscid waves. Wave-CISK was first proposed by Hayashi (1970) in order to explain certain features of tropical cloud bands. The most unstable gravity wave modes were found by Lindzen (1974) to have horizontal scales of ~3 km. More recently, the wave-CISK model has been modified to include the effects of wind shear (Raymond, 1975), cumulus momentum transport (Stevens *et al.*, 1977), frequency-dependent cloud heating (Hayashi, 1971) and phase-lagged heating (Davies, 1979). The latter two effects were introduced primarily in order to remedy the lack of scale-selection inherent in wave-CISK models, in which the growth rates increase monotonically with wave number. The interpretation of wave-CISK models is further complicated by the apparently strong sensitivity of the growth rate of the wave modes to the vertical profile of heating, which profile is generally specified *a priori*. Stark (1976) attempted to correct this deficiency by determining the cumulus heating in a more rigorous manner, using the cumulus parameterization of Arakawa and Shubert (1974), only to find that positive growth rates are possible only when the heating rates are unrealistically large. The reader is referred to Davies (1979) for a concise critique of the present state of wave-CISK theory.

Based upon the observation (e.g., Newton, 1950) that middle latitude squall lines are more or less aligned with the mean cloud-layer shear, we wish to construct a CISK model for two-dimensional disturbances with axes along the shear. The presence of both shear and background rotation makes possible the conversion of the kinetic energy of the base state flow to disturbance energy, and also alters substantially the vertical structure of neutral gravity-inertia waves. This latter effect is found to have a strong bearing on the nature of wave-CISK modes.

We proceed in Section 2 to develop a CISK model for two-dimensional disturbances with axes parallel to the shear. Solutions of the CISK model are discussed in Section 3 and compared with observations of squall lines in Section 4.

2. Wave-CISK in baroclinic flow

In performing the following linear stability analysis, we intentionally confine ourselves to the most simple form of the governing equations and boundary conditions, *viz.*, the inviscid, hydrostatic, Boussinesq form of the primitive equations linearized about an f plane, baroclinic flow with constant vertical and horizontal shears and constant stable stratification. The flow is bounded below by a rigid plate and above by an infinite layer of constant static stability and no vertical shear. The radiation condition is applied at the top of this layer.

The basic state is modelled after the observed flow in the vicinity of squall lines. As in Part I, the zonal flow in the lower layer contains constant vertical and horizontal shears

$$\bar{U} = \bar{U}_z z + \bar{U}_y y \quad (0 \leqslant z \leqslant H),$$

while the upper layer has no vertical shear and the same horizontal shear as the lower layer

$$\bar{U} = \bar{U}_z H + \bar{U}_y y \quad (H \leqslant z < \infty),$$

where H is the depth of the shear layer.

The equilibrium density distribution is taken to be of the form

$$\ln\bar{\rho} = \frac{\partial \ln\bar{\rho}}{\partial y} y + \frac{\partial \ln\bar{\rho}}{\partial z} z,$$

where the horizontal density gradient satisfies the condition of thermal wind balance

$$g \frac{\partial \ln\bar{\rho}}{\partial y} = f\bar{U}_z,$$

where f is the Coriolis parameter and g the acceleration of gravity. The Brunt-Väisälä frequency is defined for a Boussinesq fluid as

$$N \equiv \left(-g \frac{\partial \ln\bar{\rho}}{\partial z}\right)^{1/2},$$

and assumes the value N_l is the lower layer and N_s in the upper layer. This discontinuity in N serves to partially reflect wave energy propagating upward from the lower layer and is meant to crudely simulate the tropopause.

The linearized adiabatic Boussinesq equations for two-dimensional perturbations with axes aligned parallel to the shear were developed in Part I and combined into a single equation for the perturbation streamfunction ψ defined so that

$$v' \equiv -\frac{\partial\psi}{\partial z}, \quad w' \equiv \frac{\partial\psi}{\partial y},$$

where v' and w' are, respectively, the meridional and vertical components of the perturbation velocity. If we now include a diabatic heating term in the lower layer, the hydrostatic inviscid, Prandtl number unity limit of the streamfunction equations for the lower and upper layers become, respectively

$$\left(\frac{\partial^2}{\partial t^2}+f\eta\right)\frac{\partial^2\psi}{\partial z^2}+2f\bar{U}_z\frac{\partial^2\psi}{\partial y\partial z}+N_t^2\frac{\partial^2\psi}{\partial y^2}=\frac{\partial Q^*}{\partial y}\quad(0\leqslant z\leqslant H),\tag{1a}$$

$$\left(\frac{\partial^2}{\partial t^2}+f\eta\right)\frac{\partial^2\psi}{\partial z^2}+N_s^2\frac{\partial^2\psi}{\partial y^2}=0\quad(H\leqslant z<\infty),\tag{1b}$$

where η is the absolute vorticity $f-\bar{U}_y$, and Q^* is the Boussinesq equivalent of the diabatic heating rate, multiplied by $g/c_p\bar{T}$.

In order to illustrate the effect of shear on wave-CISK, we intentionally apply the very simple form of cumulus parameterization which has generally been used in the literature, namely, a form which relates the cumulus heating to the vertical velocity at some relatively low level, with the vertical heating profile specified. It should be recognized, however, that the phenomenon we wish to investigate is in many ways different from the tropical convective systems which have been the subject of most wave-CISK investigations, with the noteable exception of the work of Raymond (1975, 1976). Perhaps the most important distinction is between the thermodynamic environment typical of the tropics and that associated with severe convection in middle latitudes. The tropical environment is generally regarded (e.g., Arakawa and Shubert, 1974; Lord and Arakawa, 1980) as being on the average slightly unstable to cumulus clouds of a variety of sizes. The development of the clouds appears to proceed as a response to the destabilization by the large-scale flow, as embodied in the quasi-equilibrium assumption of Arakawa and Shubert (1974). The thermodynamic environment in the vicinity of strong convective storms has also received a great deal of attention in the literature (e.g., Lilly, 1975). This environment is typically highly unstable to large clouds, but by virtue of excessive dryness in middle levels and/or a low-level temperature inversion, somewhat stable to smaller clouds. The development of convection is thus more dependent on the presence of dynamical mechanisms which lift the boundary layer air to the level of free convection, while the persistence of the convective storms appears to be largely related to the availability of moisture (Fritsch *et al.*, 1976). Perhaps for these reasons, phenomena such as squall lines are usually relatively isolated in both space and time.

In view of these distinctions, we here choose to regard the middle-latitude squall line as an isolated event propagating through a potentially unstable air mass, rather than regarding it as a quasi-equilibrium process. The intensity of the convection is viewed as depending on the degree of conditional instability initially present and the rate at which existing moisture is supplied to the storms by the mesoscale flow. The latter will generally be proportional to the mesoscale vertical velocity at the top of the mixed layer. Since the squall line is an isolated event, the potential energy consumed need not be continuously replaced by surface evaporation or other processes.

The cumulus heating is therefore specified as a function of the mesoscale vertical velocity at a level z_0:

$$Q^*=N_t^2Q_0G(z)\left.\frac{\partial\psi}{\partial y}\right|_{z=z_0},\tag{2}$$

where Q_0 is a constant crudely proportional to the degree of instability to large cumulonimbus clouds and $G(z)$ is a specified vertical heating distribution function. Inherent in the above formulation is the assumption that the cumulonimbi respond instantaneously to the low-level mesoscale upward motion, which assumption depends on the relative time scales of the mesoscale and cumulus scale motions. This places an upper limit on the frequency of the mesoscale motion, though this limit will be seen to be relatively uninfluential in this case.

Note also that we allow negative heating to occur where the motion is downward at $z=z_0$. As discussed by Lindzen (1974), this is equivalent to neglecting the higher harmonics of a more realistic form which does not allow negative heating. A better cumulus model would also incorporate the sub-cloud layer cooling due to evaporation, which is a prominent feature of middle-latitude convection.

It is convenient to normalize the independent variables as

$$\left.\begin{aligned}z^*&=Hz\\ y^*&=H\,\mathrm{Ri}^{1/2}Nf^{-1}\pi^{-1}y\\ t^*&=\mathrm{Ri}^{1/2}f^{-1}t\end{aligned}\right\},\tag{3}$$

where the asterisks denote the old dimensional variables and Ri is the Richardson number of the lower layer, $N_t^2/\bar{U}_z^2$.

We now seek normal mode solutions of the form

$$\psi=\Psi(z)\exp(iKy+\sigma t),$$

where K is a dimensionless meridional wavenumber and σ is the complex dimensionless growth rate. With this substitution, (1) becomes

$$(\mathrm{Ri}^\eta/f+\sigma^2)\frac{d^2\Psi}{dz^2}+2i\pi K\frac{d\Psi}{dz}-\pi^2K^2\Psi=-\pi^2K^2Q_0G(z)\Psi|_{z=z_0}\quad(0\leqslant z\leqslant 1),\tag{4a}$$

$$(\mathrm{Ri}^\eta/f+\sigma^2)\frac{d^2\Psi}{dz^2}-\frac{N_s^2}{N_t^2}\pi^2K^2\Psi=0\quad(1\leqslant z\leqslant\infty).\tag{4b}$$

The solution of (4a) is found by the method of Green's functions, with the condition $\Psi=0$ applied at $z=0$ and a matching condition with the solution of (4b) applied at $z=1$; the solution of (4b) is found

straightforwardly with the radiation condition applied at $z = \infty$. The general form of the solution may be written

$$\Psi = \Psi|_{z=z_0}\left(\frac{\pi^2 K^2 Q_0 e^{-ir_0 z}}{r_1 s\left[\sin r_1 + \frac{i}{2}(R-1)e^{-ir_1}\right]}\right.$$
$$\times\left\{\left[\sin r_1(1-z) + \frac{i}{2}(R-1)e^{-ir_1(1-z)}\right]\right.$$
$$\times\int_0^z G(z')e^{ir_0 z'}\sin r_1 z'\,dz' + \sin r_1 z\int_z^1 G(z')e^{ir_0 z'}$$
$$\left.\left.\times\left[\sin r_1(1-z') + \frac{i}{2}(R-1)e^{-ir_1(1-z')}\right]dz'\right\}\right)$$
$$(0 \leqslant z \leqslant 1), \tag{5a}$$

$$\Psi = \left\{\Psi|_{z=z_0}\frac{i\pi K^2 Q_0(R-1)}{2r_1 s\left[\sin r_1 + \frac{i}{2}(R-1)e^{-ir_1}\right]}\right.$$
$$\left.\times\int_0^1 G(z')e^{ir_0(z'-1)}\sin r_1 z'\,dz'\right\}e^{ir_2(z-1)}$$
$$(1 \leqslant z < \infty), \tag{5b}$$

where we have used the definitions

$$s \equiv \mathrm{Ri}^n/f + \sigma^2$$
$$r_0 \equiv \pi K/s$$
$$r_1 \equiv r_0(1-s)^{1/2}$$
$$r_2 \equiv \pi K(N_s/N_t)(-s)^{-1/2} \times \mathrm{sign}[\mathrm{Im}(s)].$$

The quantity R is a complex reflection coefficient for waves impinging on the tropopause from below, and is defined

$$R \equiv \frac{r_0 + r_1 + r_2}{r_0 - r_1 + r_2}.$$

When (5a) is evaluated at $z = z_0$, the equality demands that the expression in large parentheses, evaluated $z = z_0$, be equal to unity. This provides the dispersion relation for s and K.

The vertical distribution of the cumulus heating may be estimated as a residual of the heat budget analyzed from observations of cumulus ensembles. The analyses performed by Nitta (1970), Wallace (1971), Reed and Recker (1971), and Williams and Gray (1973) all show that the heating which results from tropical cumulus convection peaks generally in the middle troposphere and is more or less symmetrically distributed around this region. These observations have been summarized graphically by Chang (1976).

Based upon these observed cumulus heating profiles, we choose for primary consideration a heating profile $G(z) = \sin\pi z$. This suffers the drawback of implying a non-zero heating below cloud base, but we have also taken the static stability to be finite in this region. We shall later show that the baroclinic modes satisfying (5a) are relatively insensitive to the vertical heating profile by obtaining solutions for the case $G(z)$ = constant. When the heating at the level $z = z_0$ is non-zero, care must be taken to insure that the heating is not large enough to overcome adiabatic cooling at this level, otherwise conditional instability of the first kind will result. With shear present, we must also be careful to exclude symmetric instability of the first kind.

With $G(z) = \sin\pi z$, evaluation of the integrals in (5a) leads to

$$\Psi = \frac{Q_0 K^2 \Psi|_{z=z_0}}{(s+K^2)^2 - 4K^2}[(s+K^2)\sin\pi z + 2iK(\cos\pi z - e^{-i(r_0+r_1)z} + Fe^{-ir_0(z-1)}\sin r_1 z)], \tag{6}$$

where

$$F \equiv \frac{r_2 + \frac{\pi}{2K}(s+K^2) + (r_0+r_1+r_2)e^{-i(r_0+r_1)}}{(r_0+r_2)\sin r_1 + ir_1\cos r_1}.$$

The associated dispersion relation is

$$(s+K^2)^2 - 4K^2 = Q_0[K^2(s+K^2)\sin\pi z_0 + 2iK^3 \times(\cos\pi z_0 - e^{-i(r_0+r_1)z_0} + Fe^{-ir_0(z_0-1)}\sin r_1 z_0)]. \tag{7}$$

a. Complete solutions of the dispersion relation

The general solution of (7) may be found for specified values of Q_0, z_0, N_s/N_t, and K by searching the complex s plane for values which satisfy the real and imaginary parts of (7). Asymptotic solutions may be found analytically for the special case of large K and $N_s/N_t \to \infty$, which corresponds to short waves trapped beneath a rigid lid. These asymptotic solutions are discussed in the Appendix. All solutions presented are for the case $z_0 = 0.1$.

The solutions of (7) fall into two general categories. When the heating amplitude Q_0 exceeds about 1.23, the growth rate is a monotonically increasing function of wavenumber which approaches a linear function at large K. Reference to the scaling (3) shows that the Richardson number dependence of the growth rate drops out when the latter is linearly proportioned to K. We have therefore reproduced, at large K, the classical wave-CISK solutions discussed, for example, by Chang (1976). At sufficiently large K, the solutions violate both the hydrostatic assumption and, more importantly, the assumed separation of cumulus and mesoscale time scales, making it necessary to account for the finite response time of cumulus convection to the large-scale environment (Davies, 1979).

When Q_0 is less than ~ 1.23, there exist growing solutions which are distinctly related to the base state baroclinity, having growth rates which scale as $f\,\mathrm{Ri}^{-1/2}$, and which attain maximum growth at a finite scale. An example of these solutions, for the case $z_0 = 0.1$, $Q_0 \sin\pi z_0 = 0.3$, $N_s/N_t = 1.0$ is presented in Fig. 1, which shows the growth rate and phase speed of the disturbances as a function of wavenumber for various values of the base state symmetric stability parameter $\mathrm{Ri}\eta/f$. The dimensional growth rate, phase speed, and wavelength may be obtained via

$$\left.\begin{aligned} \sigma_r^* &= f\,\mathrm{Ri}^{-1/2}\sigma_r \\ c^* &= HN\pi^{-1}c \\ L^* &= 2NHf^{-1}\,\mathrm{Ri}^{1/2}K^{-1} \end{aligned}\right\}. \qquad (8)$$

Examination of the above scaling and Fig. 1 shows that the disturbances have a distinctly mesoscale character. In fact, the Rossby number of the disturbance, defined

$$\mathrm{Ro} \equiv \frac{c^*}{\eta L^*} \approx \frac{K}{[(\eta/f)\,\mathrm{Ri}]^{1/2}}$$

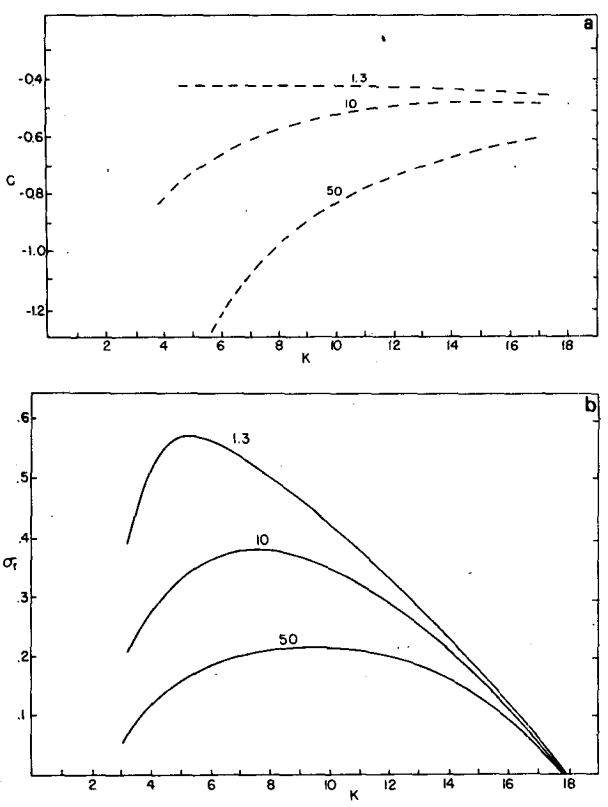

FIG. 1. Nondimensional growth rate (a) and phase speed (b) of baroclinic wave-CISK disturbances as a function of normalized wavenumber K for the case $Q_0 \sin\pi z_0 = 0.3$, $z_0 = 0.1$, and $N_s/N_t = 1.0$. Negative phase speeds denote propagation toward the warm air. The curves are labelled with values of the symmetric stability index $\mathrm{Ri}\eta/f$. See text for normalizations.

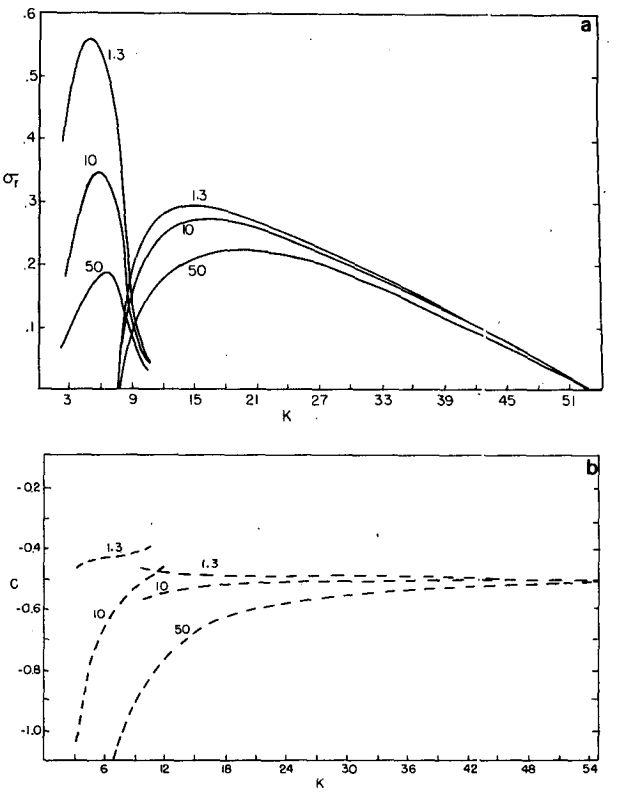

FIG. 2. As in Fig. 1 but for $N_s/N_t = 3.0$.

is order unity for values of K and $\mathrm{Ri}\eta/f$ at which the growth rate peaks. The baroclinic wave-CISK modes are thus dynamically mesoscale.

Growing solutions exist only when c is negative, indicating in this case southward propagation, or more generally, propagation toward the warm air. The phase speeds converge toward -0.5 as K increases, indicating (see the Appendix) that these modes have a phase speed and structure similar to that of free mesoscale gravity waves of total vertical wavelength H. For low values of the symmetric stability or for large values of K, the waves are nearly nondispersive. Larger growth rates are attained when the symmetric stability is small, especially when K is small.

When the ratio of stratospheric to tropospheric stabilities (N_s/N_t) is increased to reflect the presence of a tropopause, part of the wave energy is reflected at the discontinuity. This effect is observed to introduce a multiplicity of new modes, whose growth rates increase with N_s/N_t. The two most rapidly growing modes are depicted in Fig. 2, which pertains to the same parameters as Fig. 1, except that $N_s/N_t = 3.0$.

Note that the peak growth rate associated with the long-wave mode in Fig. 2 is nearly the same as that shown in Fig. 1, but that a second peak now exists at higher wavenumber. The long-wave peak is very sensitive to the symmetric stability parameter,

while the short-wave peak is less so. Where the two modes overlap, their phase speeds are nearly, but not exactly, equal.

As one increases the value of N_s/N_t, the amplitude of the peak growth rate as well as the wavenumber of maximum growth of the short-wave mode increases, and the short-wave cut-off also increases in wavenumber. The character of the long-wave mode appears to be quite insensitive to the value of N_s/N_t. Figs. 3 and 4 show the growth rates and phase speeds of the two most unstable modes for the same parameters as given for Fig. 1, but with $N_s/N_t = 10.0$ in Fig. 3, and 1000.0 in Fig. 4. In the latter case, the tropopause is effectively a rigid lid and the asymptotic analysis described in the Appendix is valid at large K. These asymptotic solutions are shown on the right-hand side of Fig. 4. Also shown is a third, northward-propagating mode which is present for very large values of N_s/N_t.

As indicated by the asymptotic analysis, an infinity of southward-propagating modes, and a single northward-propagating mode exist when a rigid lid is present and K is asymptotically large. The majority of these modes have very small growth rates and very high vertical wavenumber components and are not judged to be of much interest here. When N_s/N_t is reduced to the value in Fig. 2, all but a few of the southward-propagating modes have vanished, and the northward-propagating mode has a very small growth rate. When $N_s/N_t = 1.0$, only a single mode remains.

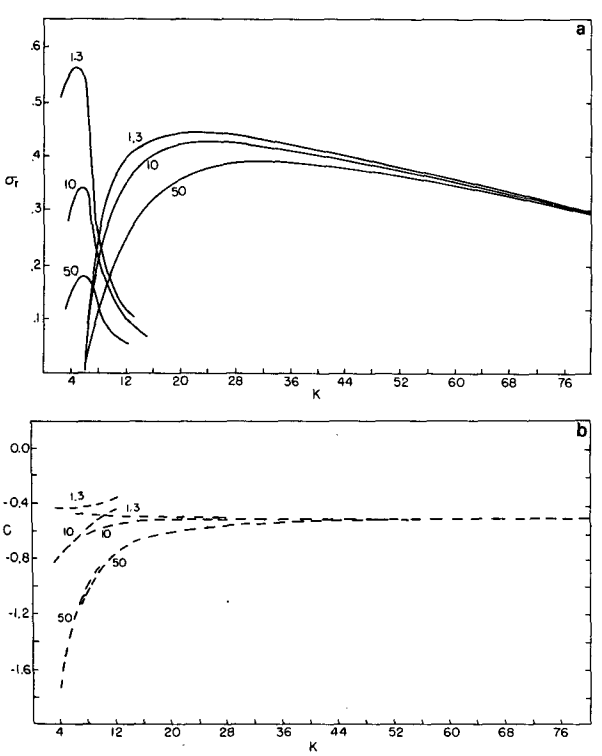

FIG. 3. As in Fig. 1 but for $N_s/N_t = 10.0$.

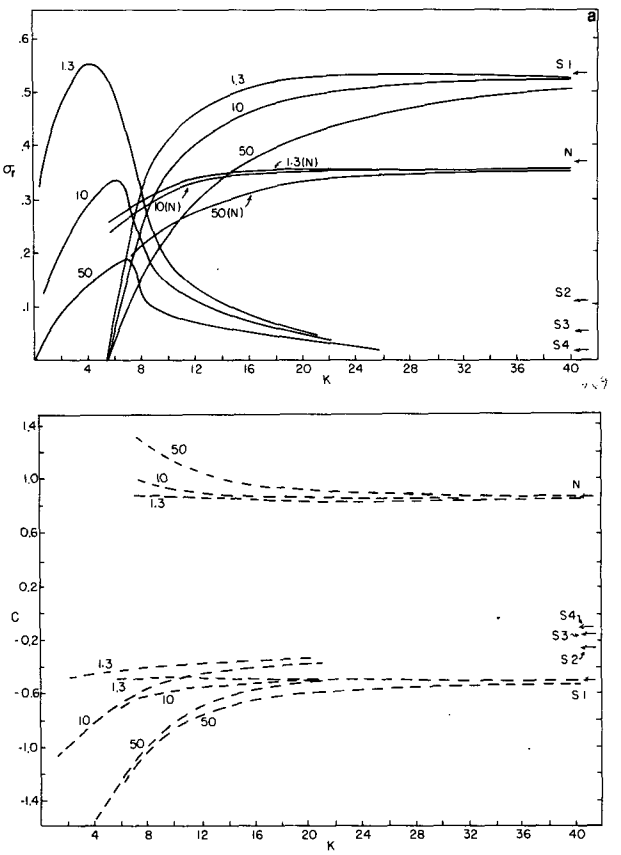

FIG. 4. As in Fig. 1 but for $N_s/N_t = 1000.0$. N denotes northward-propagating mode, and asymptotic solutions derived in the Appendix are represented by arrows at extreme right. Sn corresponds to the nth southward-propagating mode.

We now focus on the solutions when N_s/N_t is fixed at a value of 3.0, which is crudely representative of atmospheric conditions. Fig. 5 shows the growth rates of the most rapidly growing modes for the case $\mathrm{Ri}\eta/$

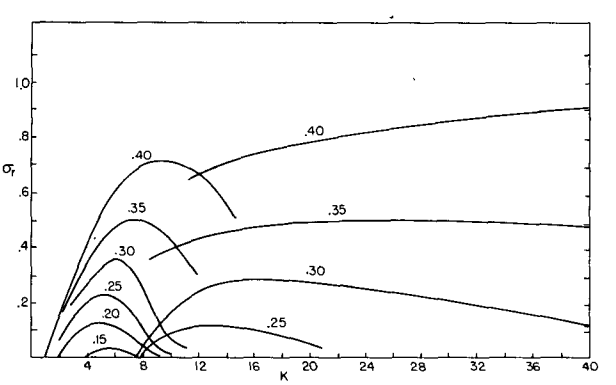

FIG. 5. Nondimensional growth rate as a function of the normalized wavenumber for various values of the cumulus heating magnitude and $z_0 = 0.1$, $N_s/N_t = 3.0$, and $\mathrm{Ri}\eta/f = 10.0$. Curves are labeled with values of $Q_0 \sin\pi z_0$.

$f = 10.0$ and $z_0 = 0.1$, and for various values of the cumulus heating. The growth rate when $Q_0 \sin\pi z_0 = 0.4$ increases without bound with K, since this heating is supercritical with respect to classical barotropic wave-CISK. As the heating diminishes, the growth rates decrease and the shortwave mode vanishes altogether when $Q_0 \sin\pi z_0$ is less than ~ 0.20. The longwave peak apparently may exist for values of $Q_0 \sin\pi z_0$ exceeding 0.12.

For purposes of comparison, the value of Q_0 can be crudely estimated from budget studies of cumulus convection. Here, since we have allowed negative as well as positive heating, we have overestimated the total production of wave energy by heating by roughly a factor of two.

Reed and Recker (1971) have estimated both the vertical velocities and diabatic heating rates which characterize synoptic-scale wave disturbances in the equatorial western Pacific. In the convectively disturbed regions of these waves, typical values of the maximum tropospheric diabatic heating and vertical velocity at the 1 km level are 6°C day^{-1} and 1 cm s^{-1}, respectively. In terms of Q^*, and accounting for the aforementioned factor of two, this is equivalent to 1.1×10^{-4} cm s^{-3}. Using (2) and assuming a tropospheric lapse rate of 3°C km^{-1}, we obtain a value of 1.14 for Q_0 and when $z_0 = 0.1$, $Q_0 \sin\pi z_0 = 0.35$. Since the sub-cloud layer of typical middle-latitude severe storm episodes is on the average a little drier than the boundary layer of the tropical Pacific, one would expect the cumulus heating to be somewhat less for an equivalent amount of convergence in extratropical systems. This is crudely consistent with the choices of Q_0 we have used in the calculations displayed in Figs. 1–4.

b. Eigenfunctions

When s has been determined from (7), the streamfunction may be obtained from (6) and (5b), while the perturbation values of buoyancy, zonal velocity, and pressure may be determined from the original set of linearized equations (see Part I), *viz.*

$$\left.\begin{aligned} B &= \left(-\frac{d\Psi}{dz} - i\pi K\Psi + i\pi K Q_0 \sin\pi z \Psi|_{z=z_0}\right)\Big/\left(s - \mathrm{Ri}\,\frac{\eta}{f}\right)^{1/2} \\ u &= \left(-\frac{\eta}{f}\mathrm{Ri}\,\frac{d\Psi}{dz} - i\pi K\Psi\right)\Big/\left(s - \mathrm{Ri}\,\frac{\eta}{f}\right)^{1/2} \qquad (0 \leqslant z \leqslant 1) \\ p &= \left(\Psi - \frac{is}{\pi K}\,\frac{d\Psi}{dz}\right)\Big/\left(s - \mathrm{Ri}\,\frac{\eta}{f}\right)^{1/2} \end{aligned}\right\}, \tag{9a}$$

$$\left.\begin{aligned} B &= -i\pi K\,\frac{N_s^2}{N_t^2}\,\Psi\Big/\left(s - \frac{\eta}{f}\mathrm{Ri}\right)^{1/2} \\ u &= -\mathrm{Ri}\,\frac{\eta}{f}\,\frac{d\Psi}{dz}\Big/\left(s - \frac{\eta}{f}\mathrm{Ri}\right)^{1/2} \qquad (1 \leqslant z < \infty) \\ p &= -\frac{is}{\pi K}\,\frac{d\Psi}{dz}\Big/\left(s - \frac{\eta}{f}\mathrm{Ri}\right)^{1/2} \end{aligned}\right\}, \tag{9b}$$

where the above quantities have been normalized by

$$\left.\begin{aligned} B^* &= N_t H^{-1} B \\ u^* &= \mathrm{Ri}^{-1/2} H^{-1} u \\ p^* &= \rho_0 N_t p \end{aligned}\right\}. \tag{10}$$

The asterisks denote dimensional values and ρ_0 is the mean density. The normalized quantities have the dimensions of the streamfunction.

Fig. 6 shows the eigenfunctions derived from (9a) and (9b) corresponding to the shortwave growth rate peak in Fig. 2, with $Q_0 \sin\pi z_0 = 0.3$, $N_s/N_t = 3.0$, $\mathrm{Ri}\eta/f = 10.0$, and $K = 16.5$. The eigenfunctions are displayed as meridional cross-sections spanning one complete horizontal wavelength and extending from the surface to $z = 1.6$. The disturbances propagate toward the left (south) in these diagrams.

The structures of the instability in the lower and upper halves of the troposphere differ dramatically. In the lower half, the disturbance strongly resembles a neutral mesoscale gravity wave; the wave in fact moves at a speed close to that of a gravity wave trapped between the surface and $z = \frac{1}{2}$ (see Fig. 2). The buoyancy and vertical velocity are nearly out of phase in this region.

Between $z = 1/2$ and the tropopause ($z = 1.0$), the streamfunction slopes back toward the colder air at an inclination similar to that of the base state surfaces of constant angular momentum.[2] In this re-

[2] The angular momentum, M, is equal to $a\cos\theta[U(y, z) + a\Omega\cos\theta]$, where a is the mean radius of the earth, Ω its angular velocity, θ the latitude, and $\bar{U}(y, z)$ is the zonally averaged zonal velocity. Surfaces of constant M slope with an angle α from the vertical, where $\tan\alpha = \bar{U}_z/\bar{\eta}$; thus M surfaces are nearly horizontal in baroclinic regions.

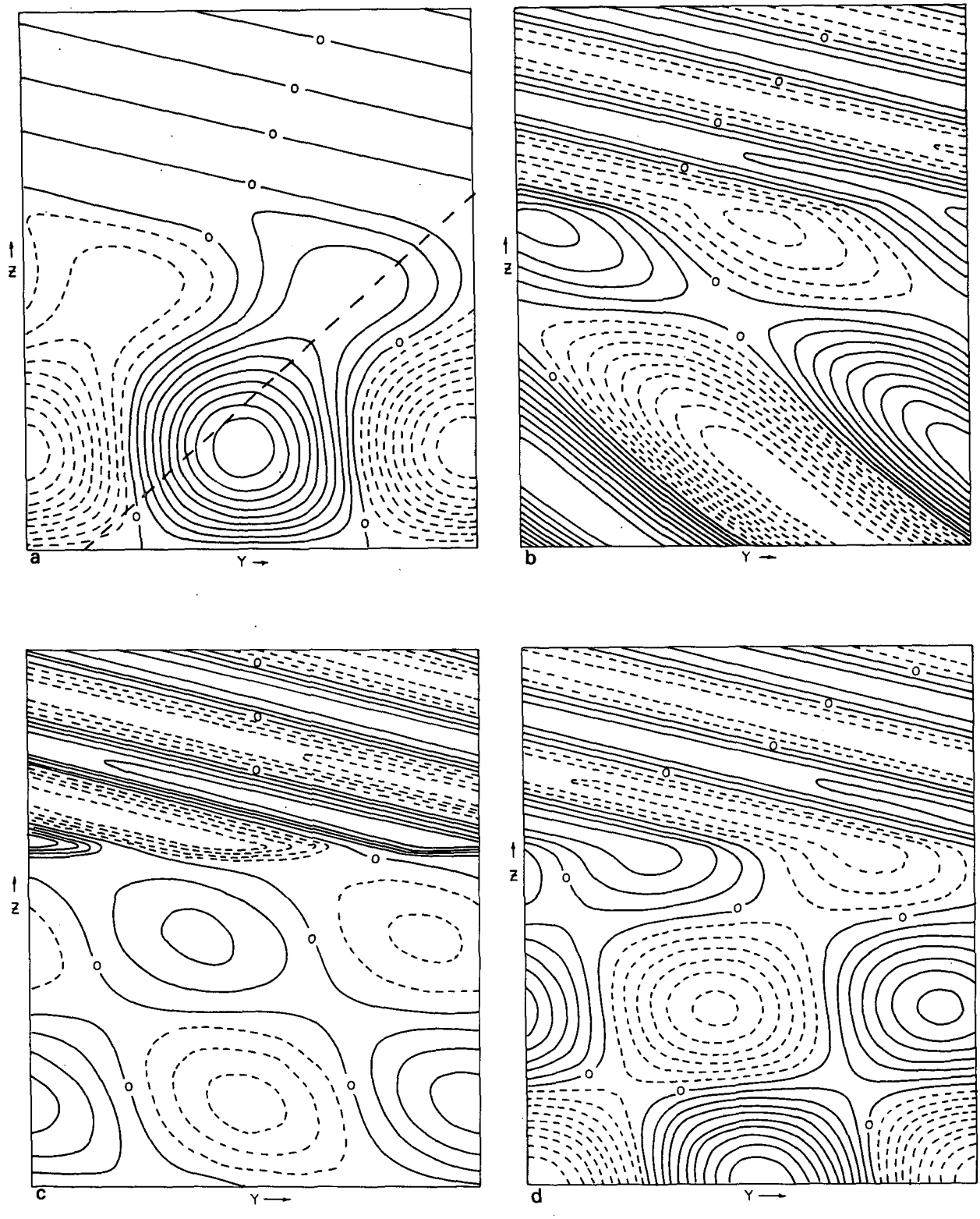

FIG. 6. Normalized eigenfunctions of the perturbation values of (a) streamfunction, (b) zonal velocity, (c) buoyancy, and (d) pressure, corresponding to the shortwave growth rate peak in Fig. 2, with $Q_0 \sin\pi z_0 = 0.3$, $N_s/N_t = 3.0$, $\mathrm{Ri}\eta/f = 10.0$, and $K = 16.5$. Fields are contoured across one full horizontal wavelength and from $z = 0.0$ to $z = 1.6$. Contour increments are one tenth of the fields' maximum values, which are: $\mathrm{Psi}_m = 1.972$, $U_m = 13.123$, $B_m = 10.762$, and $P_m = 1.554$. (In Fig. 6c, the buoyancy field is contoured at intervals of one fifth of B_m.) See text for normalizations. The heavy dashed line in (a) corresponds to a surface of constant angular momentum of the base state (see text).

spect, the flow resembles the linear response to distributed diabatic heat sources in a baroclinic circular vortex, as originally discussed by Eliassen (1951). The vertical velocity is positively correlated with buoyancy and negatively correlated with zonal velocity in this region, indicating both buoyant and

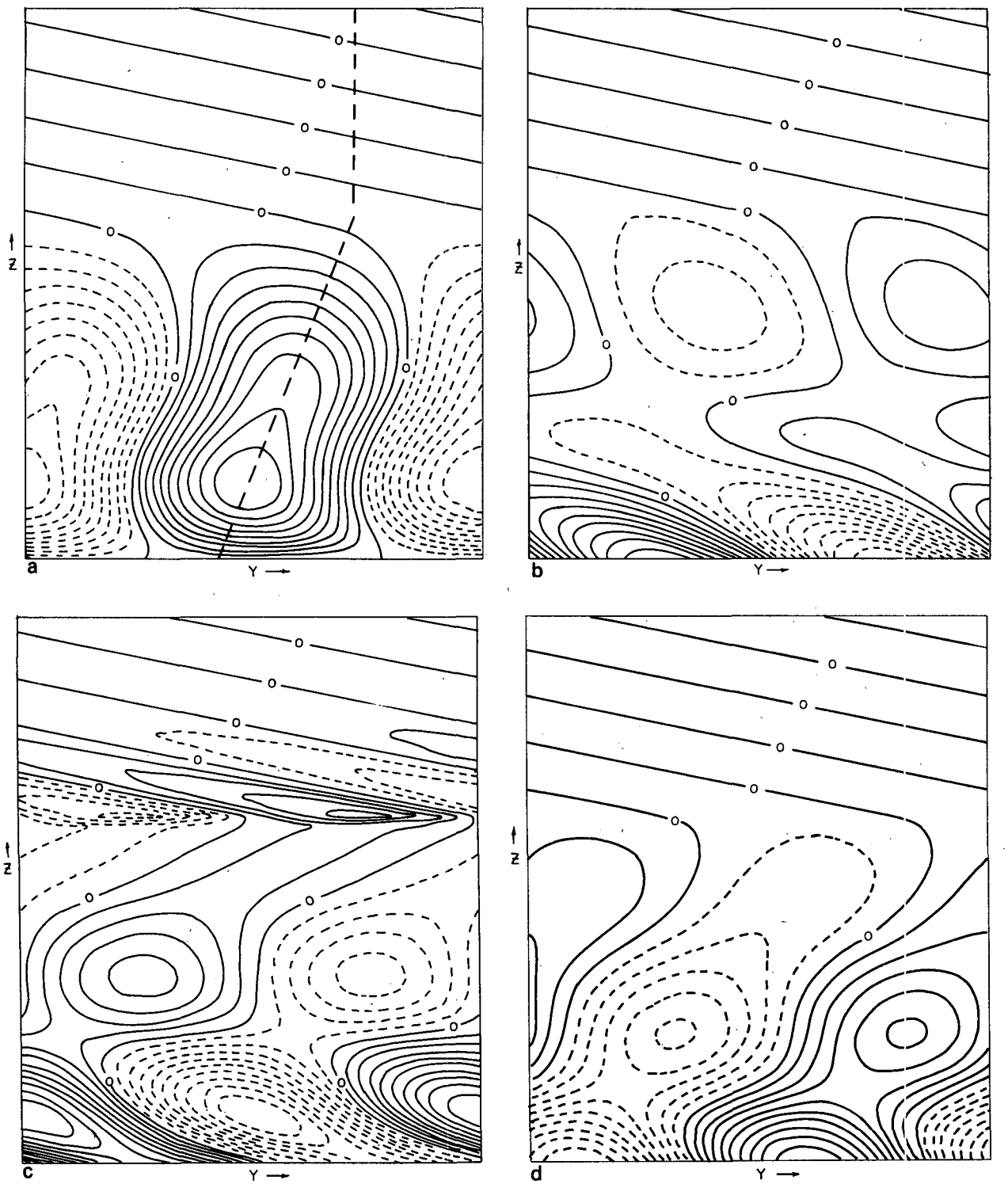

FIG. 7. As in Fig. 6, but for longwave growth rate peak in Fig.2 (K = 6.0). Psi_m = 1.407, U_m = 33.656, B_m = 4.54, P_m = 1.005.

shear production of disturbance kinetic energy. We will return to a more complete discussion of the energetics in Section 3.

An example of the structure of the long-wave mode is shown in Fig. 7, which corresponds to the same parameters as in Fig. 6, but with $K = 6.0$ (see Fig. 2). The disturbance is somewhat shallower than the short-wave instability, and less wave energy is evident in the stratosphere. The streamlines are nearly aligned with constant angular momentum surfaces through most of the troposphere; consequently the zonal velocity perturbations are weak except in the convergent layer near the surface.

The relative amplitudes of the meridional, zonal, and vertical velocities and the perturbation buoyancy and pressure may be estimated using (10). For the conditions associated with the perturbations shown in Figs. 6 and 7, and setting $N = 10^{-2}$ s^{-1}, $H = 10$ km, $\bar{T} = 290$ K, $f = 10^{-4}$ s^{-1} and $\rho_0 = 1$ kg m^{-3}, we find that if the meridional velocity has an amplitude of 5 m s^{-1} the amplitudes of the other quantities are as follows:

long wave (Fig. 7)	short wave (Fig. 6)
$w^* = 9.5$ cm s^{-1}	26 cm s^{-1}
$u^* = 19$ m s^{-1}	5.3 m s^{-1}
$T^* = 2.4$°C	4.0°C
$p^* = 1.8$ mb	2.0 mb

Under these conditions, the longwave has a period of 14 h, an e-folding time of 24 h, and a wavelength of 1050 km, while the shortwave has a period of 6.5 h, an e-folding time of 31 h, and a wavelength of 380 km.

c. *Solutions for the case G(z) = constant*

In order to determine the sensitivity of the baroclinic wave-CISK modes to the vertical heating profile, it is useful to compare the preceding results to solutions for an essentially different heating profile. We will proceed by examining solutions to the dispersion relation found from (5a) for the case $G(z) = 1.0$. The solution of (5a) for this case is

$$\Psi = Q_0\Psi|_{z=z_0}[1 + e^{-ir_0z}(\chi \sin r_1 z - e^{-ir_1 z})] \quad (0 \leq z \leq 1), \tag{11}$$

where

$$\chi \equiv \frac{(r_0 + r_1 + r_2)e^{-ir_1} - r_2 e^{ir_0}}{(r_0 + r_2)\sin r_1 + ir_1 \cos r_1}.$$

The associated dispersion relation is

$$1 - Q_0[1 + e^{-ir_0z_0}(\chi \sin r_1 z_0 - e^{-ir_1 z_0})] = 0. \tag{12}$$

The solutions of (12) are found to be quite similar to those of (7) when the *peak* values of the heating profile are the same. Fig. 8 shows the growth rates and phase speeds calculated from (11) for the case

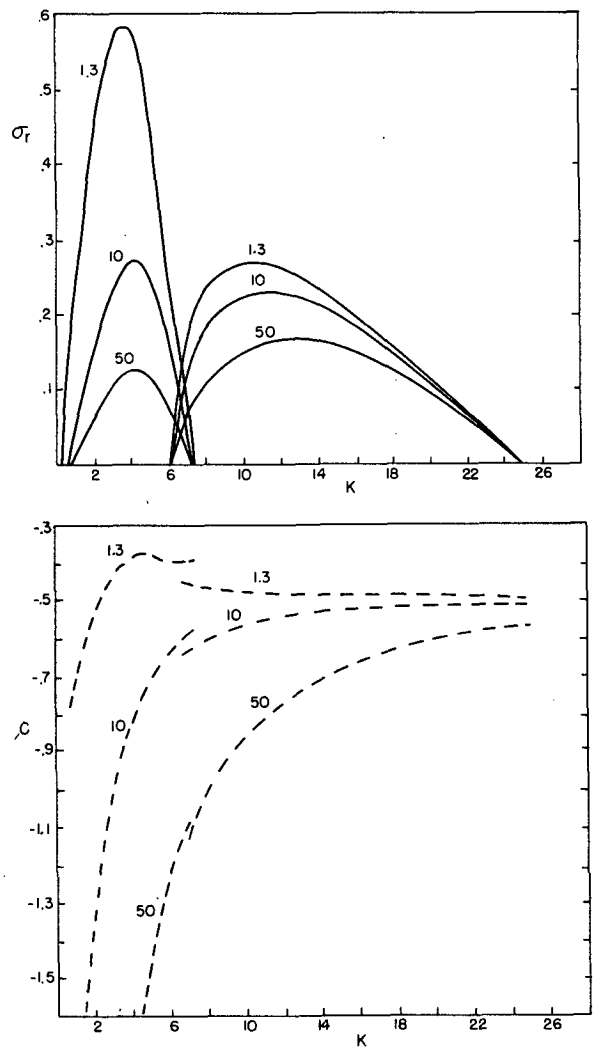

FIG. 8. As in Fig. 2, but for the case $G(z)$ = constant = 0.971. This corresponds to the peak value of the heating in Fig. 2.

$Q_0 \sin \pi z_0 = 0.3$, $z_0 = 0.1$, and $N_s/N_t = 3$. These solutions should be compared with those presented in Fig. 2, which is calculated for the same peak heating rate. The growth rates and phase speeds are similar, but the wavenumbers are generally smaller when $G(z)$ is constant. Apparently, only the wavelengths of the baroclinic modes are sensitive to the form of the heating profile, as long as the maximum heating rate is held constant.

3. Discussion

The addition of baroclinity to the wave-CISK problem appears to greatly increase the parameter range in which unstable solutions are possible. In addition to the classical barotropic modes, new baroclinic modes appear which have mesoscale time and length scales. In this section we investigate the dynamics of these baroclinic modes and discuss the

possible limitations imposed by the idealized base state.

a. *Wavelengths*

When a rigid lid is present (Fig. 4), the behavior of the growth rates as functions of the wavenumber resembles that of the classical inviscid symmetric instability (e.g., Stone, 1966) in that a longwave cutoff exists at scales such that the Rossby number is order unity, and the approach to maximum growth at infinite wavenumber is slow. Part I showed that the introduction of a small amount of diffusion leads to a preferred wavelength of Rossby number order unity in the symmetric instability problem. When there is an upper rigid lid in the present problem, the horizontal wavelength would likely scale the same way in the presence of diffusion in view of the similarity of the disturbance structure and growth rate behavior to the symmetric stability problem. In the absence of a rigid lid, however, another scale selection mechanism independent of diffusion is operative; namely, the short waves are strongly damped by the upward propagation of wave energy. Examination of Fig. 5 reveals that the most unstable modes and the modes which first appear as the heating is increased above its critical value have sufficiently long wavelengths that diffusion is not likely to be of any important consequence.

b. *Energetics*

The kinetic energy equation formed from the linear perturbation equations (Part I) has the form

$$\frac{\partial}{\partial t}\frac{1}{2}(\overline{u'^2}+\overline{v'^2}+\overline{w'^2}) = \overline{w'B'}-\bar{U}_z\overline{u'w'}-\bar{U}_y\overline{v'u'}, \quad (13)$$

where the overbars indicate averages over one meridional wavelength and over the depth of the fluid. The first term on the right represents buoyant production while the second two terms represent transfer of kinetic energy from the mean flow to the eddies. For simplicity, the generation due to horizontal shear will be neglected in this discussion.

In order to compare the buoyant and shear generation, we define a flux Richardson number, R_f:

$$R_f \equiv \frac{\overline{w'B'}}{-\bar{U}_z\overline{u'w'}}.$$

Using (10), we can write R_f in terms of the normalized perturbation quantities:

$$R_f = Ri\,\frac{Re[\widetilde{\widetilde{B(i\Psi)^c}}]}{-Re[\widetilde{\widetilde{u(i\Psi)^c}}]},$$

where the superscript c denotes the complex conjugate and the wavy overbar indicates a vertical average from $z = 0$ to $z = \infty$.

Since the normalized quantities are generally of order unity, it can be seen that R_f is generally proportional to Ri. This dependence is verified by calculations of R_f shown in Table 1. Both the shear and the heating contribute to energy production, as evidenced by a positive R_f, but the shear production is relatively small except at low Richardson numbers. There is thus the apparent paradox that while the growth rates of the baroclinic modes are linearly proportional to the ambient shear, the shear itself contributes little to the total energy production. The role of the shear in this case is indirect, and may be interpreted as follows:

Consider a linear neutral gravity wave propagating between two parallel plates in a flow with constant stratification and no shear. For simplicity, the wave is taken to represent the fundamental mode with an amplitude maximum halfway between the plates. Now suppose that CISK heating is imposed with the form given by (2), with $G(z) = \sin\pi z$, noting that this function happens also to correspond with the structure of the neutral gravity wave. It can easily be seen that in this special case, the heating is *everywhere* proportional to the vertical velocity, not just at $z = z_0$. Thus the only effect of the heating is to modify the effective static stability, and no growth can occur unless the heating is so strong as to render the fluid absolutely unstable. As shown by Bolton (1980), *growing propagating solutions can only occur when the heating is somewhere out of phase with the vertical velocity.*

In the case of the classical barotropic wave-CISK modes, the upper radiation condition causes the phase surfaces of the waves to slope with height, allowing the heating to decouple from the vertical velocity, except at $z = z_0$. When an upper rigid lid is applied and $G(z)$ is set equal to $\sin\pi z$, these modes disappear altogether (see the Appendix).

When baroclinity is present, the free wave modes slope with height whether or not an upper lid is applied; this slope is represented by the cross-derivative term in (1) and is proportional to the vertical shear. As shown in the Appendix, this allows the heating to decouple from the vertical velocity even when an upper rigid lid is present, and is otherwise apparently

TABLE 1. Values of the flux Richardson number corresponding to the growth rate peaks in Fig. 2. The calculations are performed for $\eta/f = 1.0$, $N_s/N_t = 3.0$ and $Q_0 \sin\pi z_0 = 0.3$.

Ri	K	R_f
1.3	5.0	0.52
1.3	15.0	0.39
10.0	6.0	19.1
10.0	16.5	8.4

sufficient to allow for positive growth rates at heating rates less than those required for classical wave-CISK. The higher-order modes present in the baroclinic case occur when the heating associated with the convergence field of one wave cycle overlaps with the buoyancy field of another. In the case of the southward-propagating modes, the phase slope induced by the vertical shear is in the opposite direction from the slope of the upward-radiating waves in the stratosphere (Figs. 6 and 7).

The reason for the sensitivity of the longwave baroclinic modes to the ambient symmetric stability is apparent from inspection of Fig. 7, in which it is seen that the forced flow tends to be aligned with surfaces of constant angular momentum. As shown in Part I, the resistence to displacements along such surfaces is proportional to the symmetric stability.

c. *Possible effects of critical levels*

In the preceding discussion, we have confined ourselves to an idealized flow in which the shear is everywhere parallel to the wavefronts. If a component of shear across the wavefronts exists, the waves may have one or more critical surfaces and the linear problem is somewhat less satisfactory. Observations indicate that at least some squall lines have critical levels in the upper troposphere (Miller and Sanders, 1980). If such a level exists above the primary region of convective forcing, there exists the possibility that a high percentage of wave energy will be reflected, resulting in higher growth rates of the baroclinic modes and smaller growth of the barotropic disturbances. On the other hand, much of the wave energy may be absorbed, depending on the nature of the interaction of the wave with the critical level (Booker and Bretherton, 1967). A comprehensive treatment of baroclinic wave-CISK should consider the effects of critical levels for wave propagation.

d. *Other considerations*

One of the assumptions underlying the present theory is that the cumulus convection responds instantaneously to the mesoscale vertical velocity; this assumption will be acceptable provided the time scale of the mesoscale wave is large compared to the time scale of cumulus clouds. This assumption appears to complicate the interpretation of barotropic wave-CISK, which has the time scale of a short gravity wave oscillation. The baroclinic modes have time scales which are intermediate between the inertial and the Brunt-Väisälä periods and are therefore less suspect in this regard. For the southward-propagating modes, the time scale over which an individual parcel will be subject to the mesoscale updraft is

$$\tau_m \approx \pi/\sigma_i \approx 2\pi \, \mathrm{Ri}^{1/2} f^{-1} K^{-1}.$$

If, from Fig. 2, we use a wavenumber of 16 and $f = 10^{-4}$ s^{-1}, the above amounts to

$$\tau_m \approx 1.1 \, \mathrm{Ri}^{1/2} \text{ hours}.$$

For typical atmospheric values of Ri, this mesoscale time scale would appear to be long enough to make acceptable the assumption that the cumulus respond instantly to the mesoscale flow.

The *e*-folding time for the amplification of the baroclinic modes is approximately

$$\tau_A \approx \mathrm{Ri}^{1/2} f^{-1} \sigma_r^{-1}.$$

When $\sigma_r = 0.3$, an approximate estimate is

$$\tau_A \approx 9 \, \mathrm{Ri}^{1/2} \text{ hours}.$$

Such a growth rate is rather small, and is in fact typical of the growth rate of middle-latitude baroclinic cyclones. Higher heating rates would result in somewhat larger growth rates, but the growing modes would likely be of the barotropic variety. As discussed previously, the baroclinic modes would have considerably more influence in the presence of a wave reflecting region in the upper troposphere or lower stratosphere. Otherwise, the baroclinic wave-CISK mechanism would have to be viewed primarily as a possible means of sustaining a pre-existing mesoscale gravity wave.

Another problem which arises in applying CISK theory to atmospheric disturbances concerns the finite-amplitude nature of convection in the real atmosphere. While the theory generally assumes that cumulus heating will occur for infinitesimal displacements along a surface crudely representative of the top of the mixed layer, a perturbation of substantial amplitude is generally needed to lift parcels to their level of free convection in the atmosphere. For this reason, such phenomena as tropical cyclones are rarely observed to arise spontaneously, but rather grow from an existing circulation created by some mechanism other than CISK. It would seem reasonable to suppose that wave-CISK also depends for its initiation on pre-existing disturbances of crudely similar structure. In the case of the line-symmetric baroclinic modes discussed here, frontal circulations and gravity waves are the first plausible initiating mechanisms which come to mind. While it is generally accepted that frontal circulations may initiate convection, the ability of gravity waves to elicit a convective response is less clear. Some evidence for this mechanism has been presented by Uccelini (1975), Miller and Sanders (1980) and others.

Finally, one must question whether the baroclinic wave-CISK modes are themselves stable. While a nonlinear analysis is necessary to answer this question, certain features of the linear solutions suggest that the finite-amplitude disturbances may be unstable. The most obvious of these features is the distribution of long-line velocity, examples of which

appear in Figs. 6 and 7. A horizontal cross-section through the field reveals an alternation of easterly and westerly flow, which contains inflection points; such a flow may be unstable to barotropic waves that would presumably form in the regions of strong vorticity in the middle levels of the updraft and downdraft and propagate along the line in the direction of the shear. The existence of this instability also depends on the ratio of its time scale to that of the mesoscale wave.

4. Baroclinic wave-CISK and observations of middle-latitude squall lines

The organization of convection into lines has received considerable attention from investigators of thunderstorm phenomena. The first systematic investigation of line thunderstorms in the United States occurred during the thunderstorm Project of 1946–47 (Byers and Braham, 1949). Of 56 thunderstorms observed in Ohio during the project, 32 were imbedded in lines, only six of which were associated with fronts. Byers (1951) notes that squall lines are generally more persistent than other forms of convection, lasting as long as 24 h. A few lines observed during the Thunderstorm Project contained as many as 50 individually identifiable thunderstorms. Some lines appear to form along preexisting fronts and then propagate eastward (Newton, 1950), while others develop in the warm air well east of cold fronts (Fulks, 1951).

The striking aspect of the large-scale environment of squall lines is the presence of a significant degree of vertical wind shear together with marked convective instability. Newton (1950 and 1963), Fulks (1951), Breiland (1958), Carlson and Ludlam (1968), Lilly (1975) and others all emphasize the relationship of severe storms and squall lines to vertical wind shear. Moncrieff and Miller (1976) show that a component of shear normal to convective lines may enhance the relative inflow and outflow and hence serve to intensify the system. While tropical squall lines may be organized in this manner, observations of squall lines in middle latitudes generally shown that the lines are more nearly parallel to the shear, at least in low levels. Squall lines often dissipate after propagating away from the region of strong shear (Newton, 1950).

The movement of squall lines has received considerable attention in the literature, with most investigators noting a strong tendency for the lines to move to the right of the mean winds in the cloud layer. (The observations reviewed were exclusively in the Northern Hemisphere.) The movement of squall lines relative to the surface appears to vary between 5 and 25 m s^{-1} with a mean of about 10 m s^{-1} (Boucher and Wexler, 1961). A squall line studied by Newton (1950) moved toward the southeast at an average speed of 10 m s^{-1}, while the line itself more or less paralleled the flow up to 500 mb. The severe squall lines of 3–4 April 1974 propagated eastward at $\sim$10 m s^{-1} (Miller and Sanders, 1980).

From Fig. 2 and the scaling represented by (8), it is clear that the phase speeds of the baroclinic wave-CISK disturbances will be on the order of 15 to 20 m s^{-1} or smaller, depending on the depth of the shear layer. This speed is close to the observed propagation of squall lines, but is also representative of a wide variety of propagating hydrostatic gravity waves.

Other mechanisms describing the propagation of squall lines have been proposed. The most frequently mentioned mechanism involves the horizontal spreading of rain-cooled air at the surface behind the updraft. The convergence at the leading edge of the cold air is thought to continually regenerate convection. While there is little doubt that this process is important in squall line systems, Newton (1950) notes that the advance of rain-cooled air is probably insufficient to maintain the squall line, primarily because the air behind the line is not often observed to move as fast as the line. It is also noted that large areas of rain-cooled air continue to advance into potentially unstable air long after the squall line has dissipated. Newton (1950) proposed that the propagation results from the vertical transport of horizontal momentum by convective clouds. The resulting geostrophic imbalance gives rise to a circulation which favors new convective development in regions downshear and on the warm air side of the shear. This mechanism is precisely the same as that operating in baroclinic wave-CISK, although the former is described in terms of convective rather than mesoscale momentum transports. Our description differs from Newton's only in so far as we have interpreted the effect in terms of a horizontal phase shift of the mesoscale wave with altitude.

There appears to be a remarkable association between squall lines and strong mesoscale pressure disturbances. These are most noticeable at the surface when the air adjacent to the ground is stably stratified, but are less prominent for the more typical circumstance of an adiabatic daytime boundary layer. As noted by Newton (1950), warm sector squall lines often extend north of the surface warm front into a region where the surface air is stably stratified. In these instances it is sometimes possible to detect traveling pressure waves using surface observations. A remarkable example is discussed by Brunk (1949), who was able to trace a high amplitude pressure wave as it traveled eastward from Oklahoma to New England in a region north of a surface warm front. The amplitude of the surface fluctuation was as large as 8 mb; this was accompanied by strong winds from the east. While the disturbance was originally localized in the vicinity of

a line of thunderstorms, it thereafter out-paced the latter as both moved eastward. A tendency of the pressure disturbance to move faster than the attendant squall line is also noted by Tepper (1950) and Miller and Sanders (1980); the pressure waves studied in these cases moved at 25 m s^{-1} and 15 m s^{-1}, respectively. Pressure amplitudes are generally on the order of several millibars.

In instances where the pressure wave appears to be coupled with the region of precipitation, a distinct phase relationship may be noted in which a low pressure area precedes the onset of precipitation by several hours. Hoxit *et al.* (1976) find that these troughs may be located several tens or hundreds of kilometers ahead of the convection. The onset of precipitation is foreshadowed by a pressure rise which is sometimes abrupt, while the pressure often falls again after the squall line has passed. These relationships are particularly well-illustrated in the work of Miller and Sanders (1980), who note that the pressure and wind oscillations are consistent with those of an internal gravity wave, and are thus similar to the fluctuations produced near the ground by baroclinic wave-CISK. While the pressure rise which occurs in the vicinity of the convection is probably largely a consequence of evaporative cooling of the surface air (Fujita, 1955), the pressure falls preceding the convection by several hundred kilometers demand an explanation in terms of mesoscale processes, as noted by Hoxit *et al.* (1976).

As an illustration of the relationship between strong vertical wind shear and squall lines, a vertical cross-section was constructed across several of the severe squall lines which occurred in the central United States on 3–4 April 1974. Fig. 9 shows isentropic surfaces and isotachs of the component of flow normal to the cross-section, which was constructed from four rawinsoundings. Also shown are a measure of the local symmetric stability and the positions of two squall lines. It is evident that these lines were located in regions of relatively small Richardson number associated with strong vertical wind shear. Similar cross-sections constructed through squall lines of the same outbreak have been constructed independently by Miller and Sanders (1980) and are shown in Fig. 10. According to these authors, the southeasternmost line in Fig. 10b began to dissipate shortly after the time of the cross-section and as the line moved out of the region of strong shear. (It should be noted that vertical shear is necessary to the maintenance of individual severe storms (Lilly, 1975) as well as squall lines.) The lines were observed to move east- and southeastward at a mean speed of 10 m s^{-1}.

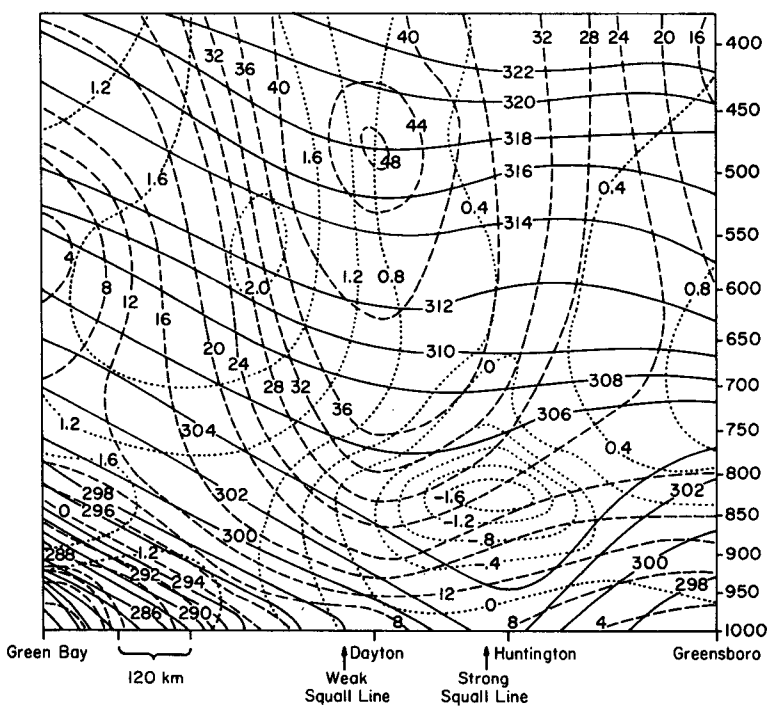

FIG. 9. Cross-section from Green Bay, Wisconsin to Greensboro, North Carolina at 0000 GMT 4 April 1974 constructed from four rawinsoundings. Solid lines are isentropes (K), dashed lines are isotachs of the component of wind into the cross-section (m s^{-1}), and dotted lines are values of a symmetric stability index $\eta/f - 1/\mathrm{Ri}$. Positions of squall lines indicated at bottom.

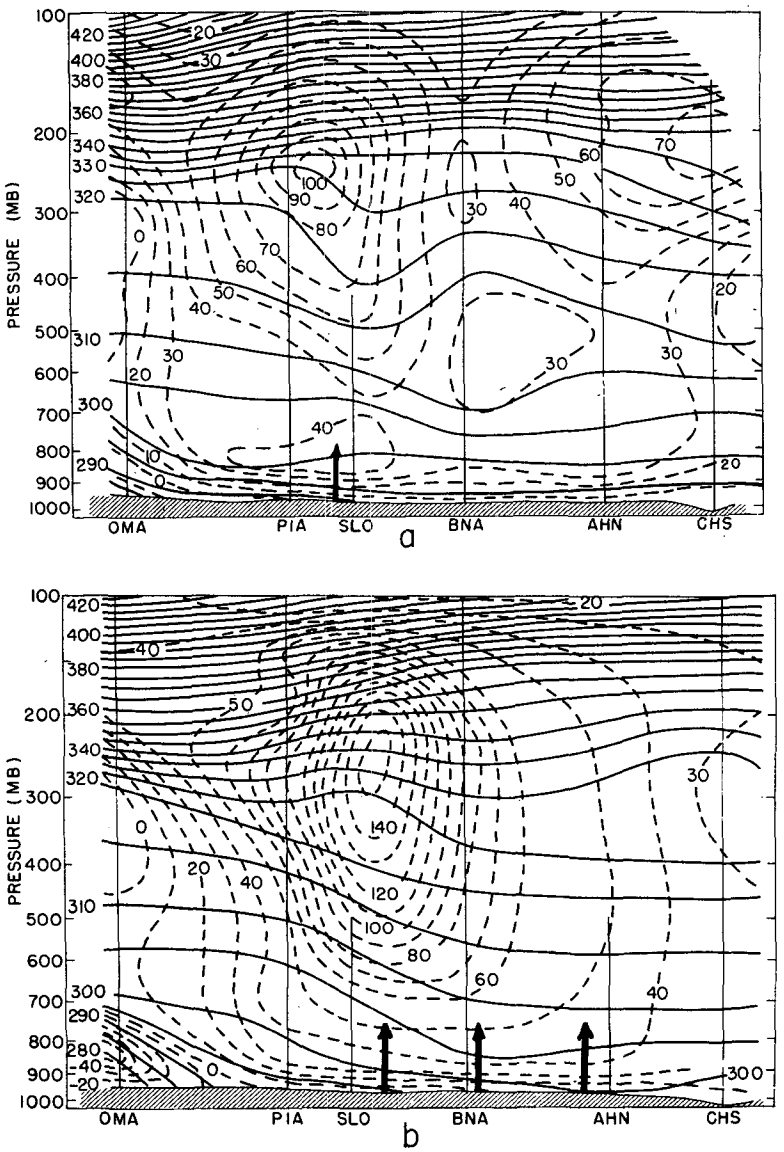

FIG. 10. As in Fig. 4 but for (a) 1200 GMT 3 April and (b) 0000 GMT 4 April 1974; wind speeds are in knots. Cross-sections are from Omaha, Nebraska, to Charleston, South Carolina. Thin vertical lines show the extent of the wind soundings; wind estimates are supplemented by geostrophic estimates near the core. Approximate positions of squall lines are shown by heavy arrows directed upward from the ground (from Miller and Sanders, 1980).

5. Conclusions

The addition of vertical wind shear and associated horizontal temperature gradients to the wave-CISK formulation has been shown to introduce new wave modes which have mesoscale length and time scales. The growth rates of these modes are proportional to the wind shear and the amount of cumulus heating, but the characteristics of the waves are relatively insensitive to the specified vertical structure of the heating. There exists a multiplicity of baroclinic modes; the two most important appear to be a mesoscale mode which is not strongly sensitive to the ambient symmetric stability, and a long-wave mode which is. Both modes propagate toward the warm air at speeds characteristic of gravity waves confined to the lower half of the forcing region.

Kinetic energy production by the baroclinic modes is made possible by the horizontal phase shift of the waves with height. This phase shift, which is due to Coriolis acceleration acting on vertically displaced parcels in conditions of vertical wind shear, allows

the cumulus heating and the wave vertical velocity to be horizontally out of phase. When the heating and velocity are out of phase, the buoyancy and vertical velocity may be partially in phase, leading to kinetic energy generation. The classical barotropic modes, on the other hand, have heating and vertical velocity fields which are necessarily in phase horizontally, unless either an upper radiation condition or a phase-lagged response is included in the formulation. The barotropic modes are highly sensitive to the vertical profile of cumulus heating.

The symmetric baroclinic wave-CISK modes described here are proposed as an explanation of a class of extratropical squall lines which form in regions of strong vertical wind shear and which have wave fronts which are roughly parallel to the shear. The observed propagation of these lines toward the warm air and their associated pressure and wind fields are well in accord with the theoretical predictions of the linear theory, although the latter fails to account for the decoupling of the pressure wave and the convective clouds which is sometimes, though not always, observed. The predicted growth rates are rather small when compared with the observations. It is hoped that some of the discrepancies between the observed and predicted behavior of squall lines can be reduced by constructing a model with more realistic initial conditions, including shear across the wavefronts and with a better convective parameterization which accounts for vertical momentum transport and sub-cloud evaporative cooling.

Acknowledgments. The author wishes to thank Mimi Dittman of U.C.L.A. and Isabelle Kole of M.I.T. for drafting the figures and Joel Sloman of M.I.T. for assistance in preparing the manuscript. Figs. 6 and 7 were prepared using the small computer operated by the Mesoscale Research Section of the National Center for Atmospheric Research.[3]

APPENDIX

Asymptotic Behavior for Large K When an Upper Rigid Lid is Present

The wave-CISK dispersion relation (7) does not generally contain any easily accessible analytic solutions. A special case arises in the limit of infinite stratospheric stratification ($N_s/N_t \to \infty$), which is analogous to a rigid lid at $z^* = H$. In this case, (7) reduces to

$$(s + K^2)^2 - 4K^2 = Q_0K^2\left[(s + K^2)\sin\pi z_0 + 2iK\left(\cos\pi z_0 + \frac{e^{ir_0(1-z_0)}\sin r_1 z_0 - e^{-ir_0 z_0}\sin r_1(1 - z_0)}{\sin r_1}\right)\right]. \quad \text{(A1)}$$

[3] NCAR is sponsored by the National Science Foundation.

Asymptotic solutions of the above may be found for large K, though it is required by virtue of the hydrostatic assumption and the scaling (3) that

$$K \ll \mathrm{Ri}^{1/2}Nf^{-1}\pi^{-1}.$$

For most atmospheric conditions, the above may be satisfied even while K is large compared to unity.

The asymptotic solutions when K is large are found to fall into two sets. The first can be found straightforwardly by assuming that

$$\lim_{K\to\infty}\begin{cases} S_r = -aK^2 \\ S_i = bK, \end{cases} \quad \text{(A2)}$$

while requiring that

$$|\sin r_1| \sim O(1).$$

In the limit of large K, the real and imaginary parts of (A1) become, respectively,

$$1 - a = Q_0 \sin\pi z_0$$

and

$$2b(1 - a) = Q_0\left\{b\sin\pi z_0 + 2\left[\cos\pi z_0 + \frac{\sin r_1 z_0 - \sin r_1(1 - z_0)}{\sin r_1}\right]\right\},$$

while inspection of the definition of r_1 shows that

$$\lim_{K\to\infty} r_1 = \frac{K\pi}{|s_r|^{1/2}} = \frac{\pi}{|a|^{1/2}}.$$

Solving the above system for a and b, we find

$$a = 1 - Q_0 \sin\pi z_0 \quad \text{(A3)}$$

and

$$b = \frac{2}{\sin\pi z_0}\left(\cos\pi z_0 + \frac{\sin r_1 z_0 - \sin r_1(1 - z_0)}{\sin r_1}\right),$$

with

$$r_1 = \frac{\pi}{(1 - Q_0 \sin\pi z_0)^{1/2}}.$$

Using (A2) and the definition of s, we may solve for the growth rate σ_r and the frequency σ_i

$$\left.\begin{aligned} \sigma_i &= \pm a^{1/2}K \\ \sigma_r &= \tfrac{1}{2}ba^{-1/2}\,\mathrm{sign}(\sigma_i) \end{aligned}\right\}. \quad \text{(A4)}$$

Several aspects of this solution are worth commenting on. When $z_0 = 1/2$, $b = 0$ and no growth is possible. This is presumably so because the symmetry of both the heating and the free modes about $z = 1/2$ prohibits the heating from decoupling with the vertical velocity. Note also that b tends to zero with Q, as expected. For $z_0 < 1/2$, which one would suspect represents the true atmosphere, $b < 0$ and in order to have positive growth rates, σ_i must also

be negative. In the large K limit, then, these growing modes will have positive phase speeds (i.e., toward the colder air) and the waves will tend toward being non-dispersive, with a dimensional phase and group velocity of

$$c^* = \frac{a^{1/2}}{\pi} NH.$$

The magnitude of the growth rate will be of order $f/\sqrt{\text{Ri}}$, thus no barotropic solutions are possible in this case.

The second set of asymptotic solutions for large K may be found by assuming that $|\sin r_1|$ is of order K^{-1} in (A1). This condition may be realized if we take

$$\lim_{K\to\infty} \begin{cases} S_r = -\dfrac{1}{4n^2} K^2 + \epsilon \\ S_i = cK, \end{cases} \tag{A5}$$

where ϵ is an undetermined parameter of order unity, and n is a positive integer. Asymptotic expansion of r_1 leads to

$$r_1 = 2\pi n + i\frac{4\pi n^3}{K} c + \left(\frac{4\pi n^3 \epsilon}{K^2} - 12\pi \frac{c^2 n^5}{K^2}\right) + O(K^{-3}).$$

Thus $|\sin r_1|$ will be at most of order K^{-1}. We now proceed to expand (A1) in powers of K and solve the real and imaginary parts separately. After some manipulation, the two parts may be solved for c and ϵ:

$$c = \frac{Q_0 \sin\pi z_0}{\pi n^3\left(1 - \dfrac{1}{4n^2}\right)\left(1 - \dfrac{1}{4n^2} - Q_0 \sin\pi z_0\right)} \tag{A6}$$

and

$$\epsilon = \frac{\pi c^2 n^3}{\sin 2\pi n z_0}\left[\frac{2c}{Q_0}\left(1 - \frac{1}{4n^2}\right) - c\sin\pi z_0 - 2\cos\pi z_0 + 3\frac{\sin 2n\pi z_0}{n\pi} + 2(1 - 2z_0)\left(\cos 2n\pi z_0 + \frac{\sin 2n\pi z_0}{nc}\right)\right]. \tag{A7}$$

Using (A5), (A6), and the definition of s, we may solve for the growth rate and frequency:

$$\lim_{K\to\infty} \begin{cases} \sigma_i = \pm\dfrac{K}{2n} \\ \sigma_r = nc\ \text{sign}(\sigma_i). \end{cases} \tag{A8}$$

Inspection of (A8) and (A6) shows that when $Q_0 \sin\pi z_0 < 3/4$, the growth rates are greatest when $n = 1$; this value will be assumed henceforth.

This set of asymptotic solutions has the same general properties as the first set, with the important distinctions that the frequency is positive and the phase speed is negative, when $z_0 < 1/2$, and the growth rates are always numerically larger. These disturbances propagate toward the warm air at a dimensional phase speed of

$$c^* = \frac{-NH}{2\pi},$$

which is smaller in magnitude than the speed of the northward propagating modes. We also note that this phase and group velocity is independent of the magnitude of the heating, unlike the northward-moving waves. For typical tropospheric conditions, c^* will be ~ 15 m s^{-1} for $H = 10$ km.

Since $|\sin r_1|$ is of order K^{-1}, its value asymptotically approaches zero for large K. Since the condition $\sin r_1 = 0$ yields the dispersion relation for free waves, it appears that the southward propagating modes represent a resonance between internal gravity waves, modified by the vertical shear, and the cumulus heating. In this case, the resonant free wave is not the gravest vertical mode; it is rather the $n = 2$ mode.

Computation of the asymptotic solutions lends credence to the numerical solution of the full dispersion relation. In Fig. 4 the asymptotic solutions for the northward-propagating mode and the four most rapidly growing southward-propagating modes are plotted on the right-hand side of the diagram. The complete numerical solutions successfully converge with the asymptotic solutions at large K.

REFERENCES

Arakawa, A., and W. H. Shubert, 1974: Interaction of a cumulus cloud ensemble with the large-scale environment, Part I. *J. Atmos. Sci.*, **31**, 674–701.

Bolton, D., 1980: Application of the Miles theorem to forced linear perturbations. *J. Atmos. Sci.*, **37**, 1639–1642.

Booker, J. R., and F. P. Bretherton, 1967: The critical layer for internal gravity waves in a shear flow. *J. Fluid Mech.*, **27**, 513–559.

Boucher, R. J., and R. Wexler, 1961: The motion and predictability of precipitation lines. *J. Meteor.*, **18**, 160–171.

Breiland, J. G., 1958: Meteorological conditions associated with the development of instability lines. *J. Meteor.*, **15**, 297–302.

Brunk, I. W., 1949: The pressure pulsation of 11 April 1944. *J. Meteor.*, **6**, 181–187.

Byers, H. R., 1951: Thunderstorms. *Compendium of Meteorology*, Amer. Meteor. Soc., 681–693.

——, and R. R. Braham, Jr., 1949: *The Thunderstorm.* Govt. Printing Off., Washington, DC, 287 pp.

Carlson, J. N., and F. H. Ludlam, 1968: Conditions for the occurrence of severe local storms. *Tellus*, **20**, 203–226.

Chang, C.-P., 1976: Vertical structure of tropical waves maintained by internally induced cumulus heating. *J. Atmos. Sci.*, **33**, 729–744.

Charney, J. G., and A. Eliassen, 1964: On the growth of the hurricane depression. *J. Atmos. Sci.*, **21**, 68–75.

Cotton, W., R. A. Pielke and P. T. Gannon, 1976: Numerical experiments on the influence of the mesoscale circulation on the cumulus scale. *J. Atmos. Sci.*, **33**, 252–261.

Davies, H. C., 1979: Phase-lagged wave-CISK. *Quart. J. Roy. Meteor. Soc.*, **105,** 325–353.

Eliassen, A., 1951: Slow thermally or frictionally controlled meridional circulation in a circular vortex. *Astrophys. Norv.*, **5,** 19–60.

Emanuel, K. A., 1979: Inertial instability and mesoscale convective systems. Part I: Linear theory of inertial instability in rotating viscous fluids. *J. Atmos. Sci.*, **36,** 2425–2449.

Fawbush, E. J., R. C. Miller and L. G. Starett, 1951: An empirical method of forecasting tornado development. *Bull. Amer. Meteor. Soc.*, **32,** 1–9.

Fritsch, J. M., C. F. Chappell and L. R. Hoxit, 1976: The use of large-scale budgets for convective parameterization. *Mon. Wea. Rev.*, **104,** 1408–1418.

Fujita, T., 1955: Results of detailed synoptic studies of squall lines. *Tellus*, **7,** 405–436.

——, 1981: Tornadoes and downbursts in the context of generalized planetary scales. *J. Atmos. Sci.*, **38,** 1511–1534.

Fulks, J. R., 1951: The instability line. *Compendium of Meteorology*, Amer. Meteor. Soc., 647–652.

Hales, J. E., Jr., 1979: On the relationship of 250 mb positive vorticity advection and horizontal divergence to tornado and severe thunderstorm development. *Proc. 11th Conf. on Severe Local Storms*, Kansas City, Amer. Meteor. Soc., 28–31.

Hayashi, Y., 1970: A theory of large-scale equatorial waves generated by condensation heat and accelerating zonal wind. *J. Meteor. Soc. Japan*, **48,** 140–160.

——, 1971: Instability of large-scale equatorial waves with a frequency dependent CISK parameter. *J. Meteor. Soc. Japan*, **49,** 59–62.

Hoskins, B. J., and F. P. Bretherton, 1972: Atmospheric frontogenesis models: mathematical formulation and solution. *J. Atmos. Sci.*, **29,** 11–37.

Hoxit, L. R., C. F. Chappell and J. M. Fritsch, 1976: Formation of mesolows or pressure troughs in advance of cumulonimbus clouds. *Mon. Wea. Rev.*, **104,** 1419–1428.

Lilly, D. K., 1975: Severe storms and storm systems: scientific background, methods, and critical questions. *Pure Appl. Geophys.*, **113,** 713–734.

Lindzen, R. S., 1974: Wave-CISK in the tropics. *J. Atmos. Sci.*, **31,** 156–179.

Lord, S. J., and A. Arakawa, 1980: Interaction of a cumulus cloud ensemble with the large-scale environment. Part II. *J. Atmos. Sci.*, **37,** 2677–2692.

Miller, D. A., and F. Sanders, 1980: Mesoscale conditions for the severe convection of 3 April 1974 in the east-central United States. *J. Atmos. Sci.*, **37,** 1041–1055.

Moncrieff, M. W., and M. J. Miller, 1976: The dynamics and simulation of tropical cumulonimbus and squall lines. *Quart. J. Roy. Meteor. Soc.*, **102,** 373–394.

Newton, C. W., 1950: Structure and mechanism of the pre-frontal squall line. *J. Meteor.*, **7,** 210–222.

——, 1963: Dynamics of severe convective storms. *Meteor. Monogr.*, No. 27, Amer. Meteor. Soc., 33–58.

Nitta, T., 1970: A study of generation and conversion of eddy available potential energy in the tropics. *J. Meteor. Soc. Japan*, **48,** 524–528.

Raymond, D. J., 1975: A model for predicting the movement of continuously propagating convective storms. *J. Atmos. Sci.*, **32,** 1308–1317.

——, 1976: Wave-CISK and convective mesosystems. *J. Atmos. Sci.*, **33,** 2392–2398.

Reed, R. J., and E. E. Recker, 1971: Structure and properties of synoptic-scale wave disturbances in the equatorial Western Pacific. *J. Atmos. Sci.*, **28,** 1117–1133.

Stark, T. E., 1976: Wave-CISK and cumulus parameterization. *J. Atmos. Sci.*, **33,** 2383–2391.

Stevens, D. E., R. S. Lindzen and L. J. Shapiro, 1977: A new model of tropical waves incorporating momentum mixing by cumulus convection. *Dyn. Atmos. Oceans*, **1,** 365–425.

Stone, P. H., 1966: On non-geostrophic baroclinic stability. *J. Atmos. Sci.*, **23,** 390–400.

Tepper, M., 1950: A proposed mechanism of squall lines: the pressure jump line. *J. Meteor.*, **7,** 21–29.

Uccellini, L. W., 1975: A case study of apparent gravity wave initiation of severe convective storms. *Mon. Wea. Rev.*, **103,** 497–513.

Wallace, J. M., 1971: Spectral studies of tropospheric wave disturbances in the tropical western Pacific. *Rev. Geophys. Space Phys.*, **2,** 557–612.

Williams, K. J., and W. M. Gray, 1978: Statistical analysis of satellite-observed trade wind cloud clusters in the western North Pacific. *Tellus*, **25,** 313–336.